Available at www.ComputerScienceWeb.com
POWERED BY SCIENCE DIRECT®

Medical Image Analysis 7 (2003) 403–416

MEDICAL IMAGE ANALYSIS

www.elsevier.com/locate/media

A generic framework for the parcellation of the cortical surface into gyri using geodesic Voronoï diagrams

A. Cachia[a,c,d,e,*], J.-F. Mangin[a,d,e], D. Rivière[a,e], D. Papadopoulos-Orfanos[a,e], F. Kherif[a,e], I. Bloch[c,e], J. Régis[b]

[a] *Service Hospitalier Frédéric Joliot, CEA, 91401 Orsay, France*
[b] *Service de Neurochirurgie Fonctionnelle et Stéréotaxique, La Timone, Marseille, France*
[c] *Département Traitement du Signal et des Images, CNRS U820, ENST, Paris, France*
[d] *Imagerie Cérébrale en Psychiatrie, INSERM ERM0205, Orsay, France*
[e] *Institut Fédératif de Recherche 49 (Imagerie Neurofonctionelle), Paris, France*

Abstract

In this paper we propose a generic automatic approach for the parcellation of the cortical surface into labeled gyri. These gyri are defined from a set of pairs of sulci selected by the user. The selected sulci are first automatically identified in the data, then projected onto the cortical surface. The parcellation stems from two nested Voronoï diagrams computed geodesically to the cortical surface. The first diagram provides the zones of influence of the sulci. The boundary between the two zones of influence of each selected pair of sulci stands for a gyrus seed. A second diagram yields the gyrus parcellation. The distance underlying the Voronoï diagram allows the method to interpolate the gyrus boundaries where the limiting sulci are interrupted. The method is illustrated with 12 different hemispheres.

Keywords: Brain; Cortex; MRI; Parcellation; Gyri; Sulci; Morphometry

1. Introduction

The recent advent of automatic methods dedicated to brain morphometry has attracted much interest from the neuroscience community (Ashburner and Friston, 2000; Fischl et al., 1999; Thompson et al., 2000; Chung et al., 2001; Toga and Thompson, 2002). These tools provide a new way of addressing issues related to the links between anatomy and function; they allow the study of the influence of various parameters on the anatomical *substratum*: sex, handedness (Davatzikos and Bryan, 2002; Mangin et al., 2003a), cognitive features (Maguire et al., 2000), genetic features (Thompson et al., 2001), pathology (Woermann et al., 1999; May et al., 1999), etc. Longitudinal studies of brain maturation or the ageing process have also received increasing attention (Paus et al., 1999, 2001; Good et al., 2001). While none of these tools can be considered perfect, simply because of the huge complexity and variability of brain anatomy, it is assumed that analyzing hundreds of brains overcomes the failures observed when analyzing a few.

1.1. Brain morphometry

Most of the brain anatomy analysis methods applied on a large scale rely on a *coordinate system*, which may be either three dimensional (like the well known Talairach grid; (Talairach and Tournoux, 1988)), or two dimensional, with spherical topology (for studies of cortical thickness, see (Fischl et al., 1999; Mac Donald et al., 2000; Chung et al., 2003)). With each method, the coordinate system is provided to each brain via a specific warping process. This process, called *spatial normalization*, matches as far as possible the different brains under study with a template endowed with the coordinate system. Morphometry is then performed on a point-by-point statistical basis, either on data-related features (Ashburner and Friston, 2000) for

*Corresponding author. Tel.: +33-1-6986-7813; fax: +33-1-6986-7786.
E-mail addresses: cachia@shfj.cea.fr (A. Cachia), mangin@shfj.cea.fr (J.-F. Mangin), http://anatomist.info.

1361-8415/03/$ – see front matter
doi:10.1016/S1361-8415(03)00031-8

studying relative or absolute tissue amount, or on deformation-related features (Chung et al., 2001) for comparing the spatial organization of the tissue (translation, rotation, shrinking, etc.).

This coordinate-based spatial normalization paradigm has had a tremendous impact on morphometry strategies because of its versatility. A number of different normalization algorithms, however, are used throughout the world, each potentially leading to different results (Hellier et al., 2003). For instance, the widely distributed SPM software[1] (Friston et al., 1995; Ashburner and Friston, 2000) allows the user to choose the template or the number of basis functions used to model the warping. This observation means that what is called ''spatial normalization'' is far from clear, which can be explained by the fact that nobody really knows what the gold standard is in terms of brain warping. Furthermore, nobody knows to what extent the matching of two different brains with a *continuous* deformation makes sense from an anatomo-functional point of view.

An alternative approach consists of following the classical way of performing morphometry, namely defining *anatomical structures by a segmentation method* and deriving *shape descriptors* (surface, volume, moments, etc.) and *inter-structure descriptors* (relative spatial position, connexity, etc.) that will be compared across brains. This alternative is sufficiently attractive to be applied manually (Sowell et al., 2002; Kim et al., 2000), although tedious work has to be performed, which prevents large-scale studies. The motivation behind this structure-based morphometry is that some neuroscience results highly related to brain architectural organization may be either lost during the non-perfect iconic spatial normalization or are inaccessible via a coordinate-based approach (Mangin et al., 2003b,c).

Finally, it should be noted that some morphometry approaches are *hybrid* because *local coordinate systems* are used to compute some shape descriptors. For instance, using a surfacic coordinate system dedicated to simply connected objects allows the computation of simple average distances between objects and opens the door to spherical harmonics-based measures (Gerig et al., 2001). The detection of cortical folds using two-dimensional regular meshes allows similar shape studies (Le Goualher et al., 2000; Davatzikos and Bryan, 2002). While some of the shape descriptors used in this approach are still disturbed by inter-individual variability in the definition of the local coordinate system, the fact that a dedicated system is used for each brain structure overcomes some of the problems related to the standard normalization paradigm. Global warping algorithms imply a trade-off between the constraints imposed by the different shapes embedded in the brain, which usually leads to a low-quality local coordinate system for complex structures like cortex sulco-gyral patterns.

1.2. Segmentation of cortical gyri

Image analysis methods dedicated to the cortex almost always focus on cortical folds (i.e. the sulci), because they can be defined simply using geometric properties (depth, curvature, medial axes, etc.). The usual neuroscience approach to cortical surface segregation, however, is gyrus based. A gyrus is usually considered to be a *module of the cortex* endowed with dense axonal connections throughout local white matter (Van Essen, 1997). Unfortunately, cortical gyri are relatively difficult to define from a pure geometrical point of view, even if they are assumed to be delimited by two parallel sulci.

Two directions of algorithmic research aim at providing automatic methods to perform structure-based morphometry. The first approach stems directly from the *iconic spatial normalization* scheme: a manual segmentation of the template is warped towards any new brain in order to obtain an automatic segmentation (Collins et al., 1995). While this approach gives good results for stable brain areas such as the deep nuclei, it is more questionable for the cortex (Tzourio-Mazoyer et al., 2002) because the warping algorithms are disturbed by the high inter-individual variability of the folding patterns (Ono et al., 1990; Rivière et al., 2002). Therefore, a concurrent strategy for the cortex consists of linking blind geometric parcellations with pattern recognition methods (Mangin et al., 1995b; Le Goualher et al., 1999; Lohmann and von Cramon, 2000; Rivière et al., 2002; Cachia et al., 2003; Rettman et al., 2002) in order to achieve a better definition of the sulco-gyral shapes to be compared across brains. Many other dedicated segmentation schemes have been defined for various applications (Duncan and Ayache, 2000).

No data-driven parcellation algorithm dedicated to gyral shapes has been proposed in the literature, because of the lack of gyrus geometrical definition. Therefore, a gyrus segmentation method has to rely on a preprocessing, yielding the detection of the sulci delimiting the gyri. A first possible approach would be to add some *constraints into warping algorithms* in order to impose a correspondence between these sulci (Thompson and Toga, 1996; Collins et al., 1998; Cachier et al., 2001). Thus warping of the template gyral segmentation would provide a reliable result. An alternative, proposed in this paper, consists of devising a *morphological definition of the gyri from the limiting sulci*.

Thus, the gyrus segmentation method proposed in this paper relies on a two-stage strategy. First, the main cortical sulci are automatically extracted and identified using a contextual pattern recognition method that may be viewed as a structural alternative to the brain warping approach

[1] http://www.fil.ion.ucl.ac.uk/spm/.

(Rivière et al., 2002). Second, the dual gyri are defined as patches of the cortical surface yielded by the computation of two nested Voronoï diagrams, the initial seeds of which are inferred from the identified sulcus bottom lines. The computed gyri correspond to a set of pairs of sulci provided by the user. These sulci can be chosen from the list of sulci defined by the neuroanatomist who has performed the manual identification used to train the pattern recognition system (Rivière et al., 2002). The method is generic because the user can select any pair of sulci, and because an alternative identification of the sulci can be provided either manually or automatically for a large-scale study if a learning database is constituted. Some user-friendly tools can be downloaded from http://anatomist.info to perform these manipulations.

The next section gives an overview of the main steps of the method: detection and labeling of the sulcus bottom lines (Section 2.1), transition from their 3D representations in the raw data to their 2D projections on the cortical surface (Section 2.2) and gyral parcellation of the cortical surface (Section 2.3). For a better understanding, the technical aspects are detailed separately (Sections 3 and 4). Finally, the method is applied to 12 different brain hemispheres and the results are discussed (Section 5).

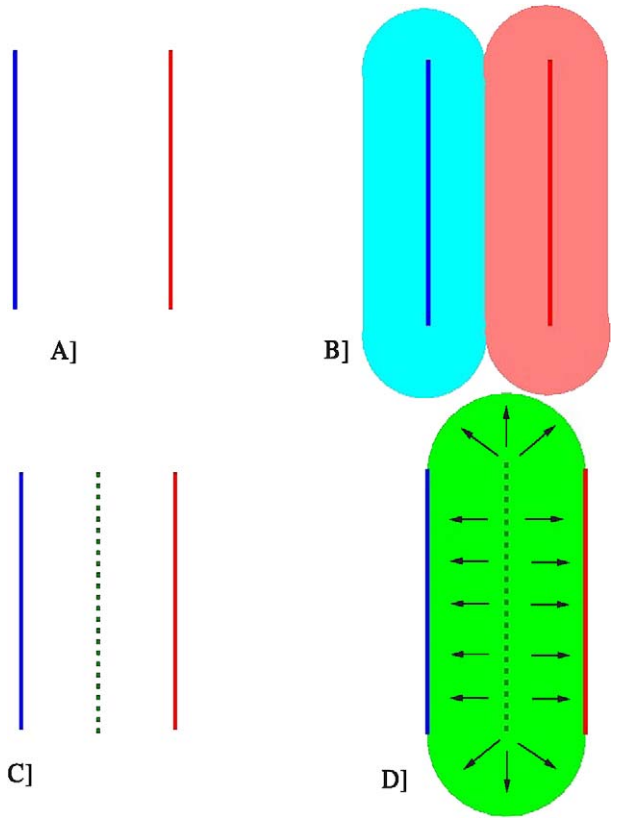

Fig. 1. Definition of a gyrus from two parallel sulci using the Voronoï diagram principle. (A) Two schematic parallel sulci. (B) Definition of the Voronoï diagram of the sulcal lines, i.e. parcellation of the domain in the zones of influence of the sulci. (C) The boundary between the two zones of influence provides the gyrus seed. (D) The gyrus delimited by the two parallel sulci can be obtained as the zone of influence of the previous boundary seed. The initial two sulcal lines must be removed from the domain to prevent the front propagation underlying the Voronoï diagram construction crossing them (a gyrus should end at the bottom of the limiting sulci). The remaining gyrus boundaries will be induced by competition with the other gyri.

2. Overview of the method

The main problem complicating the morphological definition of the gyri is the interruption of the delimiting sulci, because these interruptions are highly variable. The idea proposed in this paper overcomes this difficulty using the Voronoï diagram principle (Aurenhammer and Klein, 2000). Such a diagram is a parcellation of space from a set of seeds. Each parcel is the *zone of influence* of one of the seeds, namely the domain of space closer to this seed than to any other seed. If a set of lines approximately located at the level of the crowns of the gyri of interest can be provided as gyrus seeds, the whole gyral parcellation can be defined from a geodesic distance computed conditionally to the cortical surface. Each gyrus will be the zone of influence of its own seed (Fig. 1). In order to impose the sulcus bottoms as parts of the boundaries between these zones of influence, they are removed from the cortical surface to avoid the distances to be propagated across these lines. Hence the resulting diagram is inferred from an iterative dilation of the gyrus seeds that are stopped either at the level of the sulcus bottoms, or when two zones of influence contact each other.

2.1. Sulcus segmentation and identification

The first stage of the method, which has been described in (Rivière et al., 2002), automatically provides the identification of the main sulci, each sulcus being represented by a set of voxels obtained from a skeleton segmentation (Fig. 2). For each sulcus, discrete topology properties (Malandain et al., 1993; Mangin et al., 1995a) enable us to obtain the subset of voxels corresponding to the bottom lines (main part and branches, see Fig. 3), called *sulcal bottom lines*. Another outcome of this preprocessing stage consists of two smooth meshes of the cortex hemispheres endowed with a spherical topology (Mangin et al., 1995a, 1996), each mesh corresponding to the interface between the gray and white matter. It is onto this representation of the cortical surface that the sulcal bottom lines will be projected (cf. Section 3) to define the limits between the dual gyri. Therefore, to obtain access to the method described in this paper, the user has to provide a list of pairs of sulcus names; each pair will usually correspond to two parallel sulci, possibly interrupted, defining a gyrus.

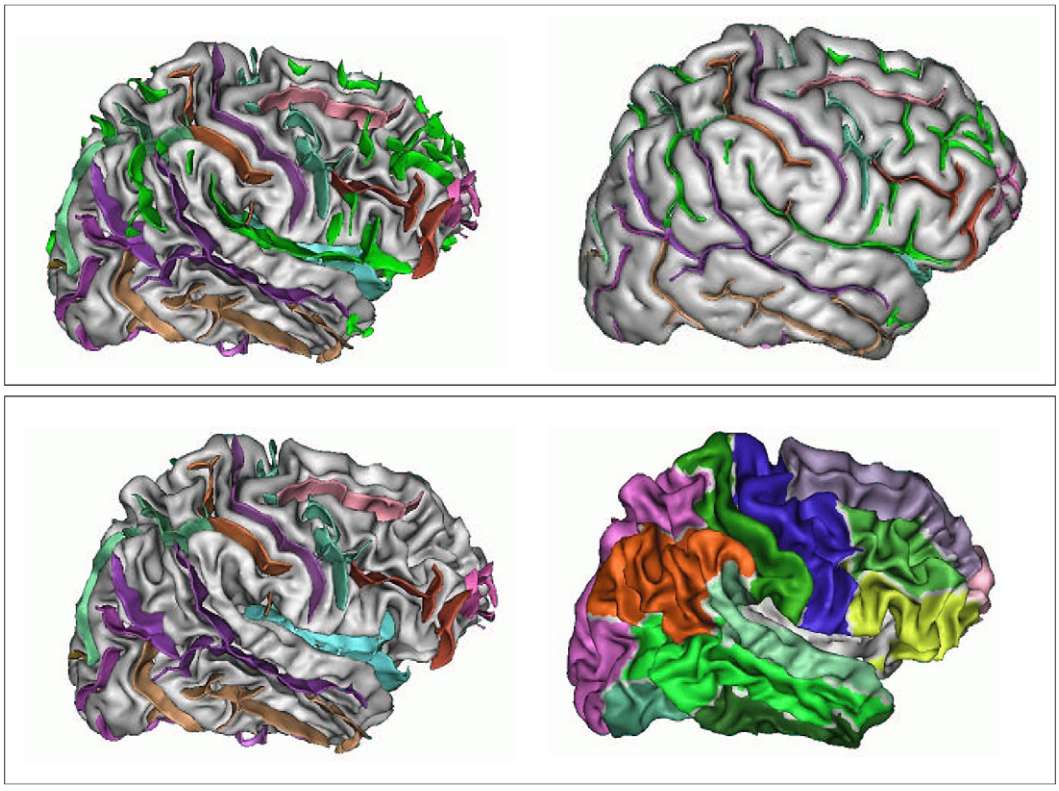

Fig. 2. Top: Result of sulcus extraction and identification (left: the white matter mesh used as a spherical model of the cortex). The different colors correspond to the various names used by our neuroanatomist to train the recognition system (Rivière et al., 2002). Bottom (left) Only the sulci used by the user as a boundary for the gyral parcellation are represented. Several small sulci, coded with the same color, have been gathered into one to create a long boundary; others, yielding useless gyral subdivisions, have been discarded. (right) The corresponding gyral parcellation. Hence, according to the user requirements, several different parcellations can be obtained using different choices of gyrus boundaries.

2.2. Projection of the sulcal bottom lines onto the cortical surface

The morphological definition of the gyri given above (see Fig. 1) assumes a processing geodesic to the cortex spherical topology. The initial sulcal bottom lines, however, are not embedded in the spherical mesh representing the cortex. Therefore, they have first to be projected into this 2D space.

To make the projected bottom lines behave like walls for geodesic distance propagation, their topology has to be preserved as far as possible during the projection. Preserving the topology during the projection process is not straightforward because of sampling differences between the initial 3D volume, in which the sulcus skeleton has been defined, and the triangulation of the cortical surface. The mesh sampling, moreover, is not regular, because it results from an adaptive decimation algorithm which adapts the size of the triangles to the local curvature.

The initial topology of the bottom line cannot be predicted because the sulcus can be interrupted, namely consist of several smaller folds and branches, the bottom lines of which do not touch each other. Hence, the projection is performed connected component by connected component.

Another important constraint is the localization of the projection that should correspond to the deepest part of the fold on the cortical surface (see Fig. 5(A)). After comparing several possible approaches (cf. Section 3.1), we chose first to project each bottom point using the tangent plane to the sulcus. Then the projection of each sulcus bottom connected component is regularized (cf. Section 3.2) in order to impose a global consistency: the whole set of bottom points is projected using the affine transformation which minimizes the squared distance to the initial projected points (Fig. 3).

Finally, morphological closing operations, processed geodesically to the triangulated surface (cf. Section 4.2), guarantee as far as possible that the projection of each connected component is a simply connected object for the mesh topology.

2.3. Gyral parcellation

Once the sulci have been projected, the remaining processing is embedded in the spherical topology of the cortical surface. The two stages of computation rely on the Voronoï diagram notion. These diagrams of zones of influence are computed via iterative dilation of the seeds

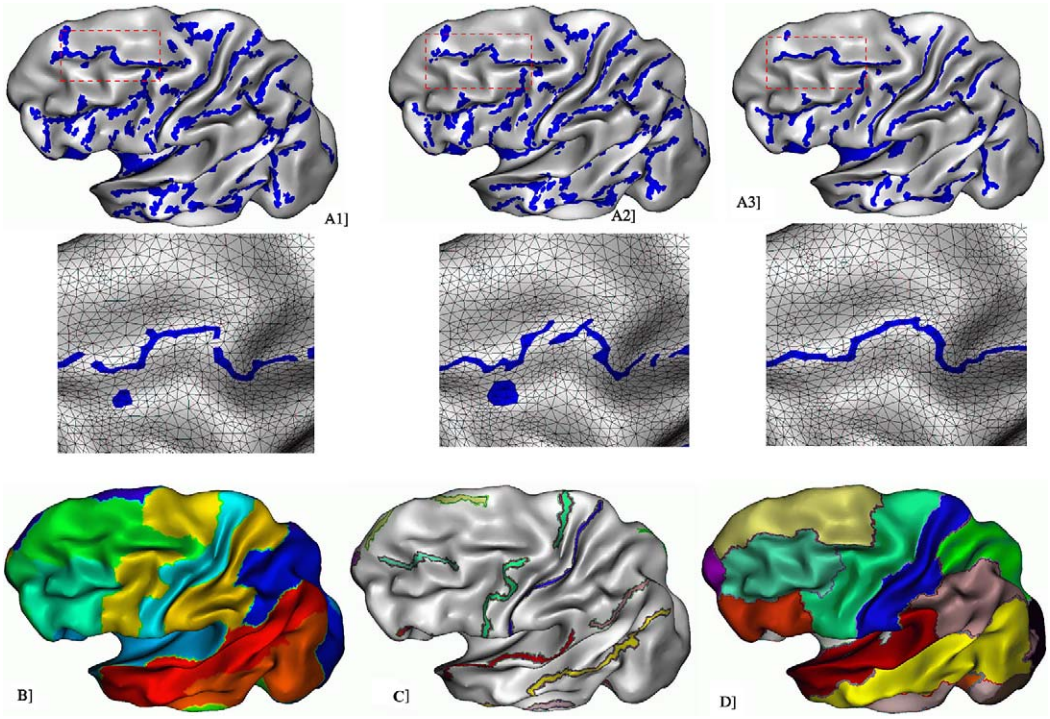

Fig. 3. A sketch of the method mapped on an inflated version of the cortical surface for clarity. Most of the remaining surface curvature is related to the gyral parcellation targeted by the algorithm. Each sulcus bottom line connected component is first projected (point-to-point (A.1), and globally using an affine transformation (A.2)). Then the projection is closed using geodesic mathematical morphology, and skeletonized in order to obtain an actual continuous line (A.3). A first Voronoï diagram is computed for the seeds corresponding to these projected lines using a geodesic distance (B). This diagram provides a sulcal-based parcellation of the surface. The seeds that will stand for the gyri are boundaries of this first diagram related to the pairs of sulci initially defined by the user (C). Finally, a second diagram is computed for these gyral seeds after removal of the sulcal seeds from the mesh in order to prevent the geodesic distance crossing a sulcus bottom (D).

according to the geodesic Euclidean distance (cf. Section 4.1).

The first step leads to the definition of a gyral seed from each pair of sulci given by the user. This definition relies on the computation of the Voronoï diagram of the labeled sulcal lines (see Fig. 3(B)).

The goal of this diagram is the detection of the boundaries between the zones of influence of the pair of sulci given by the user (see Fig. 3(C)). Such a boundary will further represent the seed of the corresponding gyrus. The set of boundaries of the diagram is sometimes called a *SKeleton by Influence Zone* (SKIZ) (Lantuejoul and Beucher, 1981). The boundaries are the nodes with at least two different labels in their direct neighborhood. Hence, the boundaries of interest are sets of nodes with exactly two labels in their neighborhood corresponding to one of the user-specified sulcus pairs (Fig. 4). This definition of the gyral seeds leads to a localization equidistant to the targeted sulcal boundaries (see Fig. 1). This localization seems to be the best one, considering that the gaps between the sulcal boundaries will be filled via competition between neighboring seeds. With this choice, the virtual boundaries will be equidistant to the midline of the two competing gyri.

The second step leads to the gyral parcellation of the cortical surface (see Fig. 3(D)). The sulcal lines are first removed from the mesh in order to prevent the dilation from crossing these targeted boundaries. Then, a Voronoï diagram is computed for the gyral seeds yielded by the previous step. Finally, this intermediary diagram is used as seed for the computation of the last diagram computed for the whole mesh, in order to fill the sulcal lines.

3. Projection of the sulcal bottom lines

The more technical part of the parcellation method is the transition from the voxel world towards the cortical spherical world. The parcellation algorithm assumes that each connected component of a sulcus bottom line can be considered as an impassable barrier. Thus, each continuous line of bottom voxels has to be transformed into a continuous line of mesh nodes. In order to achieve this result, each connected component of the sulcal bottom line is first globally projected using an affine transformation, which prevents the creation of large gaps between the projected points. The projected set is then post-processed using geodesic morphological techniques in order to obtain a simply connected line.

Because of weaknesses in the discrete topology charac-

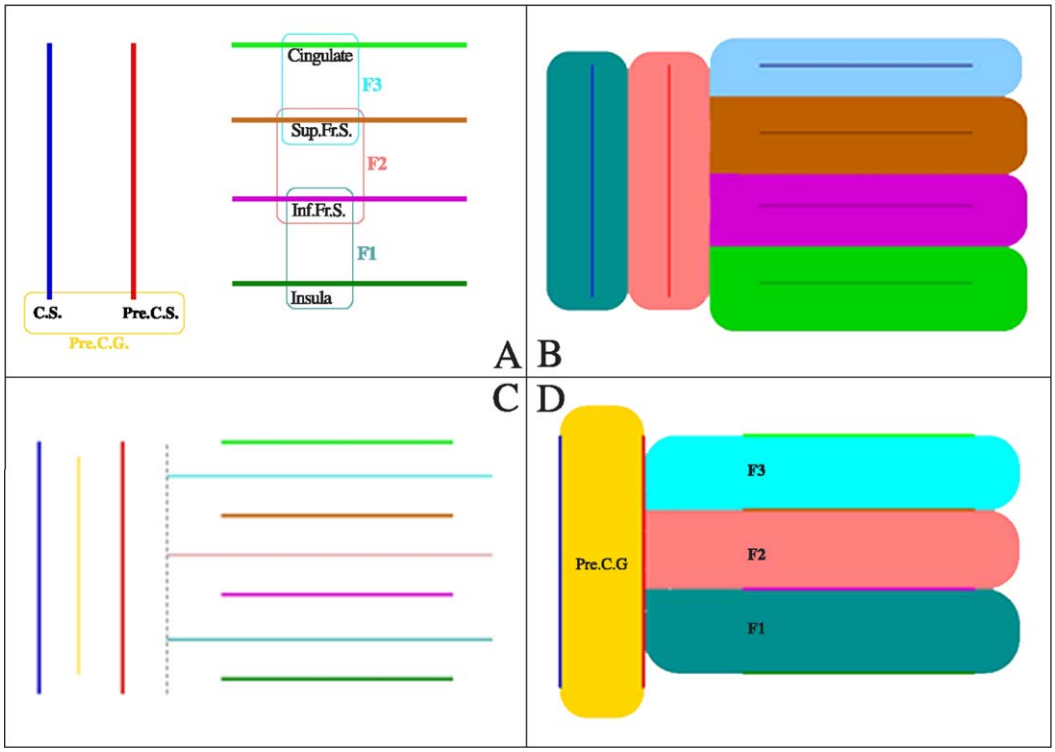

Fig. 4. Selection of the gyrus seeds. Schematic example for frontal lobe parcellation. (A) Definition of the sulcal line (C.S., Pre.C.S., etc.) of the sulci involved in a gyral pair (Pre.C.G., F1, F2, F3). (B) Definition of the Voronoï diagram of the sulcus influence zone. (C) Selection of the gyrus seeds: only the boundaries corresponding to a pair of sulci delimiting a gyrus are taken as gyrus seeds. (D) Voronoï diagram of the selected gyrus seeds. The sulcal lines are removed from the domain before the seed dilation process. The distance underlying the Voronoï diagram allows the method to extrapolate the gyrus limits where the sulci do not provide a boundary.

terization scheme used to define the bottom lines (Rivière et al., 2002), a pre-processing step has been added before their projection. Their continuity is sometimes broken because some of the *bottom points* are labeled as *junction points* (i.e. points connecting a sulcus to a branch or another sulcus). Therefore, a first volumetric closing process related to the 26-connectivities is applied to the sulcal bottom lines before projection. This closing is made up of a standard dilation followed by a homotopic erosion which preserves the topology (Malandain et al., 1993; Mangin et al., 1995a).

An important point is the choice of the geometric properties used to drive the projection process. Three different approaches have been compared to finally choose a method using the plane tangent to the sulcus surface at each bottom point. In the following, we describe first a comparison of these three point-to-point projection methods. Then, we introduce the regularized global projection, which is an adaptation of the well-known ICP algorithm (Besl and McKay, 1992; Feldmar and Ayache, 1996). Finally, we describe the geodesic post-processing.

For the sake of clarity, the following explanations

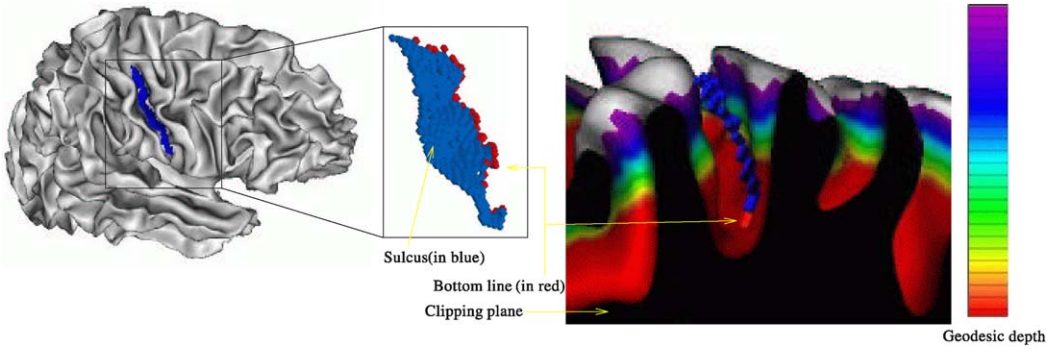

Fig. 5. Projection using local mesh information (curvature or geodesic depth). In this example, the sulcal bottom line is projected onto the cortical surface along the line of maximal geodesic distance to the gyrus crowns.

consider only one connected component of a sulcus bottom line, which is called a "sulcal line". All the processing is applied independently to each connected component.

3.1. Point-to-point matching

The algorithms described in this section projects each voxel M_i^v of the sulcal line onto a node M_i^t of the triangulation representing the cortical surface. Three different approaches have been tested, each corresponding to a different *a priori* constraint on the localization of the projected line. In each case, M_i^t is defined as the mesh node minimizing a distance to M_i^v.

3.1.1. High curvature location

In this approach, the projected sulcus bottom points are considered to correspond to high curvature locations on the spherical mesh. A high curvature is assumed to be an indicator of the exact location of the cortical fold bottom. To be more precise, since the spherical mesh is oriented, the targeted nodes are endowed with a low negative curvature. This *a priori* constraint is embedded in the definition of the distance between a bottom point M_i^v and any mesh node M:

$$d^{\mathrm{Curv}}(M_i^v,M) = d_{\mathrm{E}}(M_i^v,M) + \alpha^{\mathrm{Curv}}\,\mathrm{Curv}(M), \quad (1)$$

where α^{Curv} is a positive weighting constant, $d_{\mathrm{E}}(M_i^v,M)$ denotes the 3D Euclidean distance and Curv(M) is a curvature-related characterization of the mesh at node M. This discrete curvature is heuristically defined by

$$\mathrm{Curv}(M) = \mathrm{sign}(\overrightarrow{MB}\cdot\vec{n}_M)d_{\mathrm{E}}(M,B), \quad (2)$$

where B is the mesh neighborhood barycenter ($B = \Sigma M_i$, with M_i the neighbors of M), and $\vec{n}_M$ the normal of the mesh at node M. This heuristic is used for the smoothness of the resulting curvature map.

3.1.2. Maximal depth

In this approach, the projected sulcus bottom points are assumed to be located as deeply as possible. The deepest mesh areas are considered to correspond to the exact location of the cortical fold. As in the previous approach, this a priori constraint is included in the definition of the distance between the bottom point M_i^v and any mesh node M:

$$d^{\mathrm{Depth}}(M_i^v,M) = d_{\mathrm{E}}(M_i^v,M) + \alpha^{\mathrm{Depth}}\,\mathrm{Depth}(M), \quad (3)$$

where Depth(M) corresponds to the geodesic depth at node M. The geodesic depth computation follows the following steps (a similar approach may be found in (Rettman et al., 2002)):

1. Apply a 3D morphological closing to the white matter binary mask.
2. Apply a 3D erosion of 5 mm to the closed mask.
3. Define all the mesh nodes outside this mask as gyrus crowns. The geodesic depth of all these nodes is then null.
4. Compute the geodesic distance to these crowns, using the front propagation described below.

For the two last approaches, which embed the constraint on the localization of the projected nodes as a trade-off between the Euclidean distance and a local mesh property, the selection of the weight $\alpha^{\mathrm{Curv/Depth}}$ influences the accuracy of the projection. In practice, this weight is chosen empirically, according to the raw data resolution and the cortical mesh properties, so that the node M^t minimizing the distance $d^{\mathrm{Curv/Depth}}$ lies in the bottom of the fold, close to the voxel M_i^v.

3.1.3. Geometrical approach

In this approach, the sulcal lines are obtained as the intersection of the continuation of the sulcal surface with the cortical mesh. The sulcal surface is assumed to represent a notion closed to the medial axis of the fold, which should split the cortical surface at the right place (Fig. 6). More precisely, for each point M_i^v of the sulcal line, the tangential plane Π_i to the sulcal surface is estimated from its m_i 26 neighbors N_i^j included in the fold skeleton. It is easy to show that the normal vector $\vec{n}$ defining the best fitting tangent plane, in the sense of minimizing the sum of the squared distance of the m_i points $\{N_i^1,\ldots,N_i^{m_i}\}$ to the plane, corresponds to the smallest eigenvalue of the matrix $\Omega = \Sigma_{j=1}^{m_i}(M_i^j - M_i^v)(M_i^j - M_i^v)^{\mathrm{T}}$ (Chung et al., 2001). The projected point M_i^t of M_i^v is the closest node to M_i^v, according to the 3D

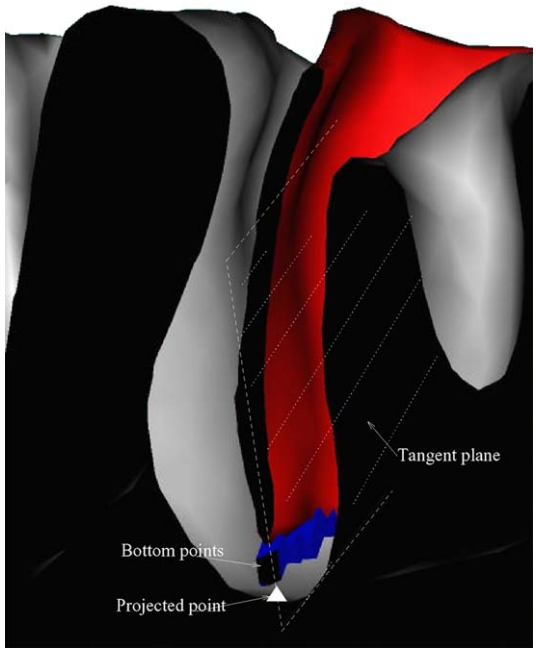

Fig. 6. Projection of the sulcal bottom line using the intersection of the plane tangent to the sulcal surface with the cortical surface mesh.

Euclidean distance, included in a stripe of 1 mm defined on both sides of the tangent plane Π_i.

3.1.4. Comparison of the three methods

Thanks to the following stages of the robust projection process, the three point-to-point projection methods introduced above generally give acceptable results. Specific configurations, however, have led us to choose the method based on the tangent plane as the most robust method. This can be understood from the fact that the assumption that the best location of the fold projection corresponds to high curvature or maximal depth of the mesh is not always verified:

- During the gyrogenesis process, some gyri are buried in the depth of the cortex and may locally fold the bottom and the walls of some sulci (Régis et al., 1995; Yousry et al., 1997; White et al., 1997; Boling et al., 1999). Such locations turn out to correspond to a minimal geodesic depth relative to the rest of the sulcus bottom (see the case of the central sulcus in Fig. 8). In fact, the bottom line of a sulcus on the mesh usually presents some depth variations. This is problematic because the distance d^{Depth} biases the projection towards depth local maxima and creates some gaps in the projection. Furthermore, the extremities of the sulcus are attracted towards the depth, which shortens the projected line. In some cases, these buried gyri also disturb d^{curv} because they present a positive surface curvature.
- Most of the time, the aspect of the folds on the white matter surface is well described as V-shaped surfaces, namely surfaces whose points with a locally minimal curvature form a single bottom line corresponding to the projection target. Unfortunately, some U-shaped sulci, whose bottom on the white matter surface is flat, can be observed. In such cases, the target line is split into two spurious lines located on both sides of the sulcus bottom. Each sulcal line point is randomly projected onto one of these two targets (Fig. 7), and the final result after regularization of the projection is not predictable.
- The definition of the geodesic depth is not a straightforward task since it requires the definition of a reference level (i.e. the null depth), which is not always clear from an anatomical point of view, especially for buried areas like the insula. When one gyrus is too buried to be included in the reference level, the line of maximal depth is ill-defined.

A comparison of the whole projection process applied to the central sulcus with the three point-to-point projection methods is given in Fig. 8. In the following results, the tangent plane method will always be used.

3.2. Robust projection

In this section, the point-to-point projection performed by the algorithm described in the previous section is regularized, mainly to minimize the width of the gaps that may exist in the middle of the set of projected points. These gaps can be created either by an erroneous estimation of the tangent plane, which can occur, for instance, because of the presence of branches along the sulcus skeleton, or because of the presence of large triangles along the bottom of a flat sulcus, which disturbs the computation of the intersection with the tangent planes.

A simple way to overcome the consequences of the problems mentioned above consists of reducing the number of degrees of freedom used to project the initial set of bottom points of the sulcal line. The point-to-point projection includes no constraint of consistency for the point set. In fact, a low-dimensional transformation should be sufficient to project the sulcal line on the mesh. Therefore, in this section, we propose to use the affine transformation

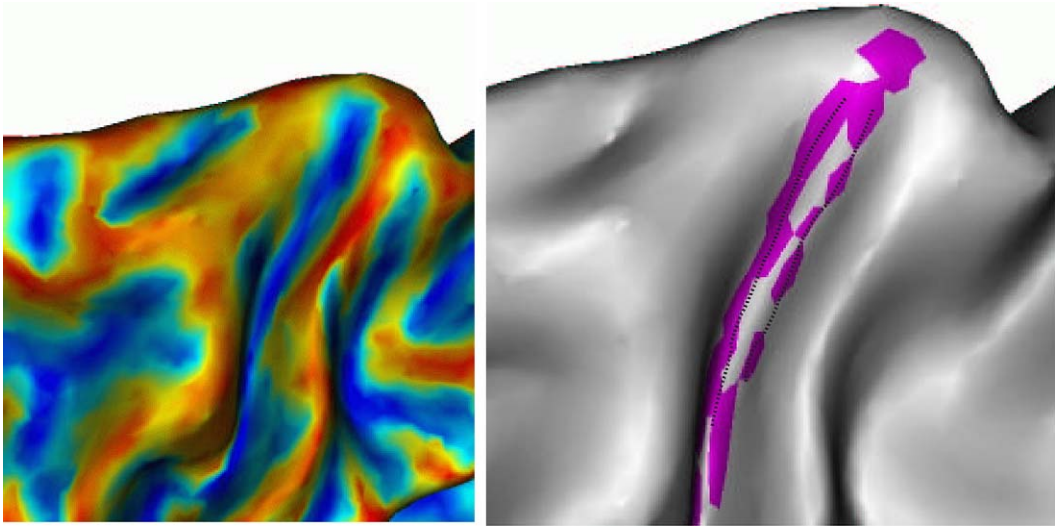

Fig. 7. Curvature information (left) and splitting of the projected sulcal line when the bottom of a fold is flat.

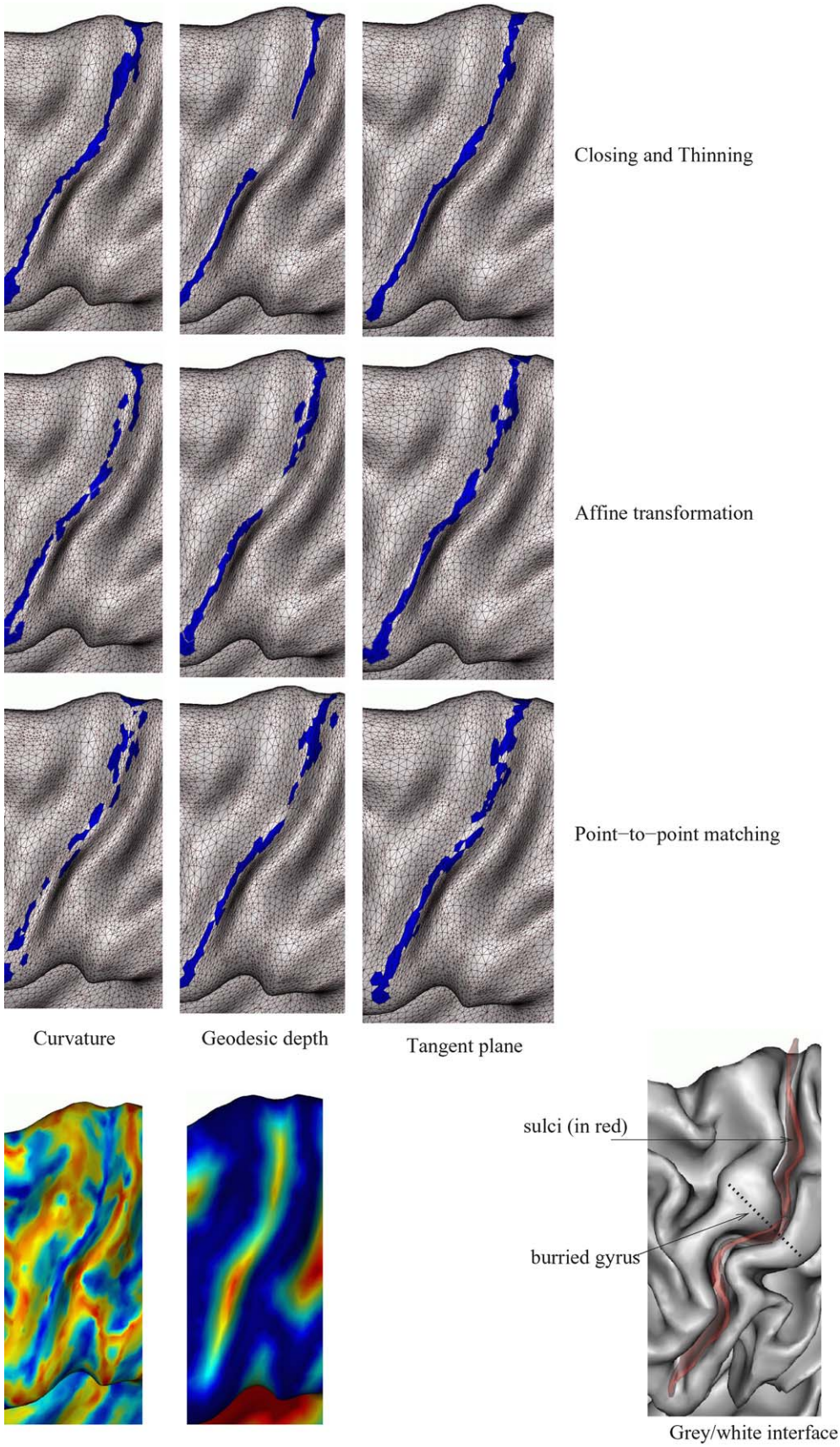

Fig. 8. Top: Projection, closing and thinning of the central sulcus. From left to right: projection using curvature, geodesic depth and a tangent plane. From bottom to top: first projection using point-to-point matching, affine transformation, closing and thinning (for the sake of clarity, the projections of the sulcal line, buried in the depth of the cortex, are mapped on an inflated version of the cortical surface). Bottom: From left to right: curvature and geodesic depth map used to drive the projection; the presence of a buried gyrus locally deforms the wall and the ridge of the central sulcus.

which minimizes the sum of the squared distances between the bottom points and their point-to-point projection. In order to obtain a robust estimation, an outlier detection method is included in a two-stage process. It should be noted that this method does not need to be very sophisticated (Huber, 1981), because some additional morphological post-processing is still required to fill the gaps appearing in the oversampled areas of the mesh. A detailed explanation of the least square estimation of the affine transformation is proposed in Appendix A. The following is the method of outlier rejection:

1. A first estimation of the affine transformation A^{init} is made after discarding the points M_i^v, whose projection M_i^t is too far away. This first outlier rejection results from a single threshold on the Euclidean distance (in practice 10 mm). Then, a new projection M_i^{init} is computed for each M_i^v as the closest mesh node to the transformed point $A^{\text{init}}M_i^v$. It is assumed that the first estimation of A^{init} is a good approximation of the final transformation. Hence, it will be used to obtain a better outlier detection.
2. A second estimation of the affine transformation A^{final} is made after discarding a fixed percentage p of the points M_i^v, which present the greatest Euclidean distance between M_i^t and M_i^{init} (in practice $p=10\%$). The goal is to discard points whose point-to-point projection is not consistent with the majority of the bottom points. This final transformation A^{final} is then used to perform the final projection of the whole set of M_i^v, the projected nodes M_i^{final} corresponding to the closest mesh node to the transformed point $A^{\text{final}}M_i^v$.

4. Morphological processing

The last stage of the projection method aims at closing the potential gaps in the projected set of points. The goal is to create a barrier for the computation of the final Voronoï diagram. This is achieved through a dilation of the projected set on the mesh of the cortical surface. The size of the dilation is the minimal size yielding a simply connected object, which is controlled from the computation of the number of connected components and the Euler number. Finally, a homotopic skeletonization preserving the topology is applied to the dilated set in order to obtain a thin line, namely a chain of nodes connected by some triangle edges.

4.1. Geodesic dilations and Voronoï diagrams

All the geodesic distances used in the method described in this paper stem from the thick front propagation idea proposed in (Verwer et al., 1989). This method is based on a special case of the A^*-algorithm (Hart et al., 1968), which provides the length $d(n)$ of the shortest path in a graph from a set of nodes S to any other node n. The white matter mesh is considered as a graph, whose edge lengths are simply their Euclidean length. The length $d(n)$ is initialized by zero for the set S and an infinite value anywhere else. Nodes are then processed in a specific order, determined by the length of the path to S. Lengths and order are calculated recursively during the search process: if n' is a neighbor of n, then $d(n')$ is upgraded by $d(n)+d(n,n')$ when it leads to a length decrease. This algorithm can be understood as the propagation of a thick front, made up of the points located in a short range of distance to the set. The front is initialized with the set S. The front is then iteratively updated by removing the closest point to S after having propagated the length to its neighbors, and adding them to the front if they had not yet been reached.

This algorithm only provides a coarse approximation of the exact Euclidean geodesic distance. Hence, it cannot be used to develop a Mathematical Morphology, because dilations cannot be composed correctly. The result, however, is sufficient to perform simple quasi-isotropic dilations, by applying a threshold to geodesic distance maps. In practice, the front propagation is stopped as soon as the threshold is reached, for the sake of efficiency. The front propagation corresponding to the dilation of the initial projected set is stopped regularly in order to check the topology of the dilated set (practically, the checking is performed each 0.5 mm).

The Voronoï diagrams are computed using the same thick front propagation algorithm, with the additional update of a label image $l(n)$. A different label is initially given to each seed. The set of seeds is the set S from which is computed the distance propagation. Each update of $d(n')$ is followed by an update of $l(n')$ by $l(n)$, which corresponds to the underlying seed dilation. When all the points of the mesh have been reached, the label image corresponds to the Voronoï diagram.

4.2. Simple points and homotopic skeletonization

The dilated projected point set, which is now simply connected, is skeletonized in order to obtain an *actual* line (i.e. a chain of node points). The skeletonization is homotopic so as to preserve the topology obtained during the previous step. Its implementation on the mesh relies on the definition of simple points in two-dimensional domains (Serra, 1982): a point of a binary image is simple, namely it can change color without topological change, if its immediate neighborhood contains exactly one white connected component and one black connected component. This characterization is used to develop the following skeletonization algorithm:

(1) Put all the nodes of the object connected to outside into the front.
(2) Mark all the non-simple points of the front as ''immortals''.
(3) Repeat until the front is empty:

(a) repeat until the front is empty:
  (i) remove the next point of the front;
  (ii) compute its topological characterization if it is not 'immortal';
  (iii) if it is a simple point, remove it from the object and update the topological characterization of its neighbors; otherwise, mark it as 'immortal';
(b) put all the nodes connected to outside into the front.

5. Results and discussion

The method has been applied to the two hemispheres of six different brains extracted from a database of brains whose sulci had been identified manually by a neuroanatomist in order to train the pattern recognition system. The list of sulcus pairs selected by the user corresponded to long neighboring parallel sulci, in order to obtain as far as possible the usual parcellation described in anatomical atlases. The results proposed in Fig. 9 share striking similarities across the six brains. More work has to be done on sulcus pair selection, however, to obtain a more intuitive parcellation.

These results are also qualitatively comparable to atlas descriptions, except for the occipital lobe. This lobe does not include gyri corresponding to our morphological definition. Comparing these results with manually defined gyri has not yet been carried out, first because it is tedious and difficult work which has to be done on a large database to be significant, and second because the parcellations yielded by our method are not intended to correspond *exactly* with the standard method. The standard cortical parcellation was proposed by anatomists 100 years ago, when the functional segregation of the brain into functional areas was not known. Thus, this standard point of view is not necessarily the only meaningful one to compare

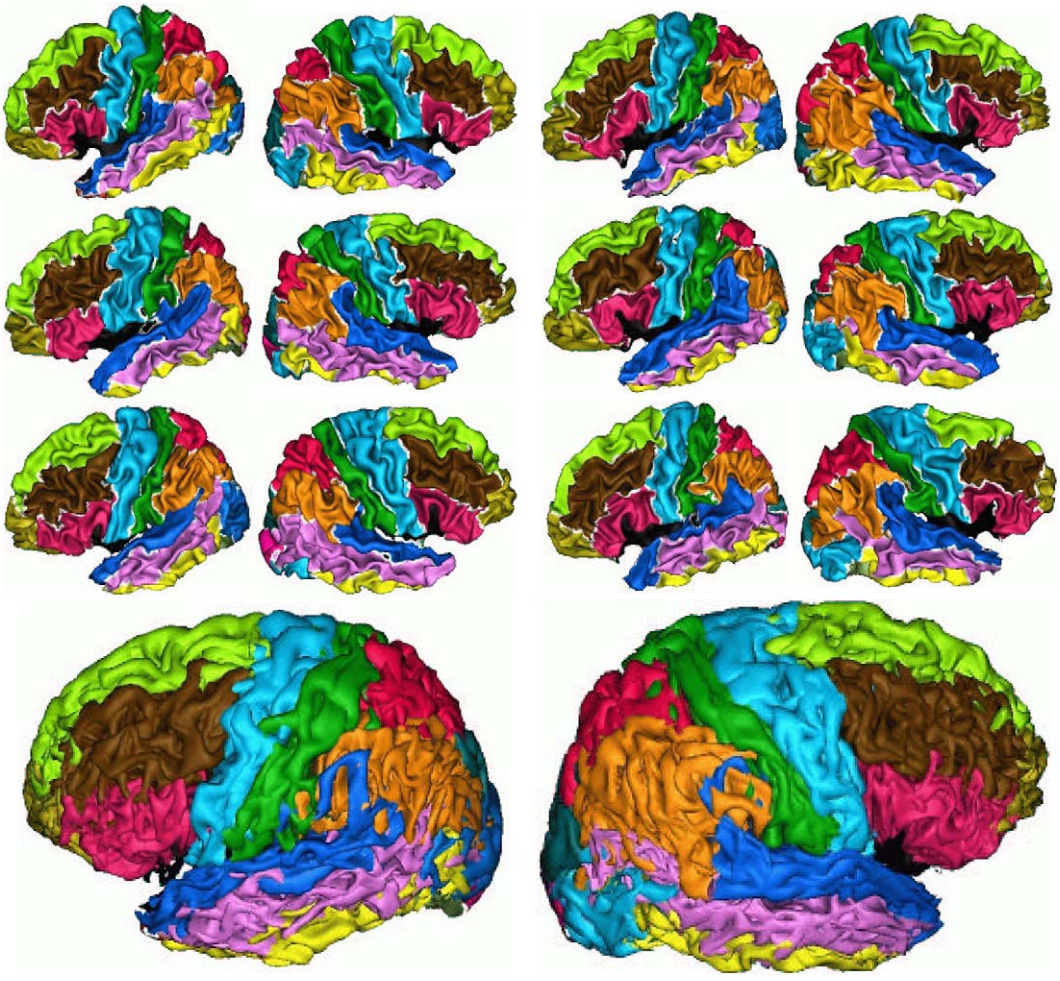

Fig. 9. A typical result obtained for the two hemispheres of six different brains. Each color corresponds to a different gyrus. The boundaries between gyri appear in white. For the external face of the brain, the set of pairs of sulci selected for this experiment aims at defining the three horizontal frontal gyri and the polar frontal face, the three horizontal temporal gyri, the pre- and postcentral vertical gyri corresponding to motor (cyan) and somesthesic (green) areas, and the two parietal lobules. Some unsatisfactory attempts were made to parcellate the occipital lobe. The lowest images provide a superimposition in the Talairach proportional system of the mesh of the six brains. Other kinds of parcellations can be obtained if the user selects a different list of sulcus pairs.

populations. The goal of the method described in this paper is to provide an automatic and reliable parcellation technique, which can be applied on large databases, using the same morphological definition for all the brains. Therefore, our efforts are aimed at searching for parcellations which can be consistently inferred from the sulcus identification, whatever the inter-individual variability of the sulco–gyral patterns.

The huge folding variability highlighted in the figure illustrates the difficulties preventing a simple geometrical definition of the gyri. Some frontal sulci that are often long non-interrupted furrows can be split into several pieces in some brains. This phenomenon disturbs both the sulcus recognition and the gyrus definition. Nevertheless, our method can extrapolate the usual parcellation to these intriguing complex configurations. Hence, any brain can be processed in a rather consistent automatic and reliable way, which opens the door to large-scale comparisons between pathological and standard subjects. According to the user's interest, different sulcus pair lists may be provided to the method in order to compare gyral areas and shapes from various definitions. One of the weaknesses of our approach, however, is the need to define a set of gyri covering the whole cortical surface or at least surrounding each gyrus of interest. Competition between neighboring gyri is mandatory in our morphological definition.

Future work will aim at extending the method to a more general morphological definition of cortical patches. The current method is dedicated to gyri delimited by two long parallel sulci. Current neuroanatomical research on the cortical folding process, however, could provide a reliable detection of smaller sulcal units called sulcal roots that may allow a finer parcellation of the cortical surface (Régis et al., 1995; Cachia et al., 2003). These units can be considered as points of the cortical surface where the folding begins. Thus, sets of such points could be used to define the limits of gyrus subunits using extensions of the idea described in Fig. 4. This extension means that the definition of each cortical patch seed will be related to a set of more than two sulcal lines, without a specific relationship, like parallelism, between them. A similar extension could be used to define lobes, which could allow us to deal with the occipital lobe, for instance (other lobes can be obtained by merging several gyri).

The direct morphometric application of our method is the comparison of the cortical patch areas between brains. Other related measures like the volume of grey matter in the gyrus can be obtained. The gyral cortical patches can be backprojected to the 3D mask of the grey matter, to be used as 3D seeds. Then, a volumetric geodesic Voronoï diagram can be computed in the cortex grey matter in order to split it into gyri. The ratio between gyrus grey matter volume and gyrus area would also provide an average cortical thickness measure. Finally, more sophisticated descriptors of the gyrus shape could be computed using, for instance, 3D invariant moments (Poupon et al., 1998).

While the first application of automatic cortical parcellation methods relies on morphometric studies, splitting the cortex into standard pieces could also be used as a referential system to compare functional results, using a volume-of-interest-based statistical method (Evans et al., 1991). Another interest in the cortical parcellations into gyral patches stems from the recent development of MR diffusion imaging for fiber tracking (Poupon et al., 2001). The methods used to detect the fiber bundles linking two different cortical areas are still in their infancy, but this new possibility may lead to the development of dedicated mapping methods. One possibility is the inference of the matrix of connectivity of the main cortical gyri. For each individual, using gyral patches as input and output may allow the sorting of the huge number of tracked bundles. Then individual matrices of connectivity could be compared on a statistical basis. This approach could provide new research and diagnostic tools for the pathologies related to brain connectivity.

6. Conclusion

The complexity and variability of the sulco–gyral patterns of the human cortex remain a challenging issue for the research field aiming at normalizing brain anatomy for brain mapping purposes. As matters stand, it is difficult to claim that a perfect solution can be reached using a warping strategy. This paper contributes to the stream of research aiming at analyzing the cortex patterns from a structural point of view closer to the neuroanatomist's approach. The parcellation method assumes that a reliable identification of the main sulci can be made first for any subject, which is far from the case with the current pattern recognition system. We believe, however, that the current state of this system is sufficient to obtain interesting morphometry results if a large database of brains is processed, which can now be done without any user interaction. This belief relies on the large number of significant results obtained by voxel-based morphometry in spite of poor spatial normalization.

Appendix A. Least square estimation of the affine transformation

In this appendix, we give the technical details leading to a least squares estimation of the affine transformation matching two set of paired 3D points $\{X^1, X^2, \ldots, X^n\}$ (the set of bottom voxels) and $\{Y^1, Y^2, \ldots Y^n\}$ (the set of nodes provided by the first *point-to-point* projection stage):

$$A \cdot X^i = L \cdot X^i + T = Y^i \quad (i = 1, \ldots, n), \tag{A.1}$$

where $X^i = [X^i_x, X^i_y, X^i_z]^{\mathrm{T}}$, $Y^i = [Y^i_x, Y^i_y, Y^i_z]^{\mathrm{T}}$, L is a linear transformation (i.e. a 3×3 real matrix) and T a translation

vector. Using condensed block matrix notation for the affine transformation, namely $\tilde{X}^i = [X^i_x, X^i_y, X^i_z, 1]^{\mathrm{T}}$ $(n \times 4)$, $Y^i = [Y^i_x, Y^i_y, Y^i_z]^{\mathrm{T}}$ $(n \times 1)$, $\tilde{A} = [L|T]$ (3×4), Eq. (A.1) can be written as

$$[\tilde{A}|\tilde{X}^1|\tilde{X}^2|\ldots|\tilde{X}^n] = [Y^1|Y^2|\ldots|Y^n] \quad (i = 1, \ldots, n). \tag{A.2}$$

The transposition of this equation yields

$$[\tilde{X}^1|\tilde{X}^2|\ldots|\tilde{X}^n]^{\mathrm{T}} \cdot \tilde{A}^{\mathrm{T}} = [Y^1|Y^2|\ldots|Y^n]^{\mathrm{T}} = \begin{bmatrix} Y^1_x & Y^1_y & Y^1_z \\ Y^2_x & Y^2_y & Y^2_z \\ \vdots & \vdots & \vdots \\ \vdots & \vdots & \vdots \\ Y^n_x & Y^n_y & Y^n_z \end{bmatrix} = [Y_x|Y_y|Y_z]. \tag{A.3}$$

If we denote $\tilde{A}^{\mathrm{T}} = [A_x|A_y|A_z]$ and $\Gamma = [\tilde{X}^1|\tilde{X}^2|\ldots|\tilde{X}^n]^{\mathrm{T}}$, Eq. (A.1) can be expressed as a separate problem, amounting to solving for each coordinate x, y and z a set of linear equations:

$$\begin{bmatrix} \Gamma A_x \\ - - - \\ \Gamma A_y \\ - - - \\ \Gamma A_z \end{bmatrix} = \begin{bmatrix} Y_x \\ - - - \\ Y_y \\ - - - \\ Y_z \end{bmatrix}. \tag{A.4}$$

Practically, the resolution of each equation $\Gamma A_j = Y_j$ $(j = x,y,z)$ is performed in a least-squares fashion, entailing for each direction x, y and z the multiplication of the pseudo-inverse matrix of the initial points Γ^- $(\Gamma^- = (\Gamma^{\mathrm{T}}\Gamma)^{-1}\Gamma^{\mathrm{T}})$ by a vector containing the coordinate of the projected points Y_j:

$$\begin{aligned} A_x &= \Gamma - Y_x, \\ A_y &= \Gamma - Y_y, \\ A_z &= \Gamma - Y_z. \end{aligned} \tag{A.5}$$

References

Ashburner, J., Friston, K.J., 2000. Voxel-based morphometry—the methods. NeuroImage 11, 805–821.

Aurenhammer, F., Klein, R. (Eds.), 2000. Voronoi Diagrams. Elsevier, Amsterdam, Chapter 5, pp. 201–290.

Besl, P., McKay, N., 1992. A method for registration of 3d shapes. IEEE Trans. Pattern Anal. Mach. Intell. 14 (2), 239–256.

Boling, W., Olivier, A., Bittar, R.G., Reutens, D., 1999. Localization of hand motor activation in broca's pli de passage moyen. J. Neurosurg. 91 (6), 903–910.

Cachia, A., Mangin, J.-F., Rivière, D., Kherif, F., Boddaert, N., Andrade, A., Papadopoulos-Orfanos, D., Poline, J.-B., Bloch, I., Zilbovicius, M., Sonigo, P., Brunelle, F., Régis, J., 2003. A primal sketch of the cortex mean curvature: a morphogenesis based approach to study the variability of the folding patterns. IEEE Trans. Med. Imaging 22 (6), 754–765.

Cachier, P., Mangin, J.-F., Pennec, X., Rivière, D., Papadopoulos-Orfanos, D., Régis, J., Ayache, N., 2001. Multisubject non-rigid registration of brain MRI using intensity and geometric features. In: Niessen, W., Viergever, M. (Eds.), 4th International Conference on Medical Image Computing and Computer-assisted Intervention (MICCAI'01), Utrecht, The Netherlands. LNCS, Vol. 2208, pp. 734–742.

Chung, M.K., Worsley, K.J., Paus, T., Cherif, C., Collins, D.L., Giedd, J.N., Rapoport, J.L., Evans, A.C., 2001. A unified statistical approach to deformation-based morphometry. NeuroImage 14 (3), 595–606.

Chung, M., Worsley, K., Robbins, S., Paus, T., Taylor, J., Giedd, J., Rapoport, J., Evans, A.C., 2003. Deformation-based surface morphometry applied to gray matter deformation. NeuroImage 18 (2), 198–213.

Collins, D.L., Holmes, C.J., Peters, T.M., Evans, A.C., 1995. Automated 3D model-based neuroanatomical segmentation. Hum. Brain Mapp. 3, 190–208.

Collins, D.L., Le Goualher, G., Evans, A.C., 1998. Non-linear cerebral registration with sulcal constraints. In: MICCAI'98. LNCS, Vol. 1496, pp. 974–984.

Davatzikos, C., Bryan, R.N., 2002. Morphometric analysis of cortical sulci using parametric ribbons: a study of the central sulcus. J. Comput. Assist. Tomogr. 26 (2), 298–307.

Duncan, J., Ayache, N., 2000. Medical image analysis: progress over two decades and the challenges ahead. IEEE Trans. Pattern Anal. Mach. Intell. 22 (1), 85–106.

Evans, A.C., Marrett, S., Torrescorzo, J., Ku, S., Collins, L., 1991. MRI–PET correlation in three dimensions using a volume-of-interest (VOI) atlas. J. Cereb. Blood Flow Metab. 11 (2), A69–A78.

Feldmar, J., Ayache, N., 1996. Rigid, affine and locally affine registration of free-form surfaces. Int. J. Comput. Vis. 18 (2).

Fischl, B., Sereno, M.I., Tootle, R.B., Dale, A.M., 1999. High-resolution intersubject averaging and a coordinate system for the cortical surface. Hum. Brain Mapp. 8 (4), 272–284.

Friston, K.J., Ashburner, J., Frith, C.D., Poline, J.B., Heather, J.D., Frackowiak, R.S., 1995. Spatial registration and normalization of images. Hum. Brain Mapp. 2, 165–189.

Gerig, G., Styner, M., Shenton, M.E., Lieberman, J.A., 2001. Shape versus size: improved understanding of the morphology of brain structures. In: MICCAI 2001. LNCS, Vol. 2208. Springer, Berlin, pp. 24–32.

Good, C.D., Johnsrude, I.S., Ashburner, J., Henson, R.N., Friston, K.J., Frackowiak, R.S., 2001. A voxel-based morphometric study of ageing in 465 normal adult human brains. NeuroImage 14 (1), 21–36.

Hart, P., Nilson, N., Raphael, B., 1968. A formal basis for the heuristic determination of minimum cost paths. IEEE Trans. Syst. Sci. Cybern. SSC-4, 100–107.

Hellier, P., Barillot, C., Corouge, I., Gibaud, B., Le Goualher, G., Collins, D., Evans, A., Malandain, G., Ayache, N., Christensen, G., Johnson, H., 2003. Retrospective evaluation of inter-subject brain registration. IEEE Trans. Med. Imaging 22 (9), 1120–1130.

Huber, P., 1981. Robust Statistics. Wiley Series in Probability and Mathematical Statistics.

Kim, J., Crespo-Facorro, B., Andreasen, N., O'Leary, D., Zhang, B., Harris, G., Magnotta, V., 2000. An MRI-based parcellation method for the temporal lobe. NeuroImage 11 (4), 271–288.

Lantuejoul, C., Beucher, S., 1981. On the use of the geodesic metric in image analysis. J. Microsc. 121, 39–49.

Le Goualher, G., Procyk, E., Collins, D.L., Venugopal, R., Barillot, C., Evans, A.C., 1999. Automated extraction and variability analysis of sulcal neuroanatomy. IEEE Med. Imaging 18 (3), 206–217.

Le Goualher, G., Argenti, A.M., Duyme, M., Baare, W.F., Hulshoff Pol, H.E., Boomsma, D.I., Zouaoui, A., Barillot, C., Evans, A.C., 2000. Statistical sulcal shape comparisons: application to the detection of genetic encoding of the central sulcus shape. NeuroImage 11 (1), 564–574.

Lohmann, G., von Cramon, D.Y., 2000. Automatic labelling of the human cortical surface using sulcal basins. Med. Image Anal. 4 (3), 179–188.

Mac Donald, D., Kabani, N., Avis, D., Evans, A.C., 2000. Automated 3-D extraction of inner and outer surfaces of cerebral cortex from MRI. NeuroImage 12 (3), 340–356.

Maguire, E.A., Gadian, D.G., Johnsrude, I.S., Good, C.D., Ashburner, J., Frackowiak, R.S., Frith, C.D., 2000. Navigation-related structural change in the hippocampi of taxi drivers. Proc. Natl. Acad. Sci. USA 97 (9), 4414–4416.

Malandain, G., Bertrand, G., Ayache, N., 1993. Topological segmentation of discrete surfaces. Int. J. Comput. Vis. 10 (2), 158–183.

Mangin, J.-F., Frouin, V., Bloch, I., Regis, J., López-Krahe, J., 1995a. From 3D MR images to structural representations of the cortex topography using topology preserving deformations. J. Math. Imaging Vis. 5 (4), 297–318.

Mangin, J.-F., Regis, J., Bloch, I., Frouin, V., Samson, Y., Lopez-Krahe, J., 1995b. A Markovian random field based random graph modelling the human cortical topography. In: CVRMed, Nice. LNCS, Vol. 905. Springer, Berlin, pp. 177–183.

Mangin, J.-F., Régis, J., Frouin, V., 1996. Shape bottlenecks and conservative flow systems. In: MMBIA, San Francisco, pp. 319–328.

Mangin, J.-F., Rivière, D., Cachia, A., Papadopoulos, D., Collins, D.L., Evans, A.C., Régis, J., 2003a. Object based strategy for the morphometry of the cerebral cortex. In: IPMI, Ambleside, UK.

Mangin, J.-F., Rivière, D., Coulon, O., Poupon, C., Cachia, A., Cointepas, Y., Poline, J.-B., Le Bihan, D., Régis, J., Papadopoulos-Orfanos, D., 2003b. Coordinate-based versus structural approaches to brain image analysis. Artificial Intelligence in Medicine, in press.

Mangin, J.-F., Poupon, F., Rivière, D., Collins, D.L., Evans, A.C., Régis, J., 2003c. 3D moment invariant based morphometry. In: MICCAI, Montreal, Springer.

May, A., Ashburner, J., Buchel, C., McGonigle, D.J., Friston, K.J., Frackowiak, R.S., Goadsby, P.J., 1999. Correlation between structural and functional changes in brain in an idiopathic headache syndrome. Nat. Med. 5 (7), 836–838.

Ono, M., Kubik, S., Abernethey, C.D., 1990. Atlas of the Cerebral Sulci. Georg Thieme.

Paus, T., Zijdenbos, A., Worthley, K., Collins, D.L., Blumenthal, J., Giedd, J.N., Rapoport, J.L., Evans, A.C., 1999. Structural maturation of neural pathways in children and adolescents: in vivo study. Science 283, 1908–1911.

Paus, T., Collins, D.L., Evans, A.C., Leonard, G., Pike, B., Zijdenbos, A., 2001. Maturation of white matter in the human brain: a review of magnetic resonance studies. Brain Res. Bull. 54 (3), 255–266.

Poupon, C., Mangin, J.-F., Clark, C.A., Frouin, V., Régis, J., LeBihan, D., Bloch, I., 2001. Towards inference of human brain connectivity from MR diffusion tensor data. Med. Image Anal. 5, 1–15.

Poupon, F., Mangin, J.-F., Hasboun, D., Magnin, I., Frouin, V., 1998. Multi-object deformable templates dedicated to the segmentation of brain deep structures. In: MICCAI'98, MIT. Springer, Berlin, pp. 1134–1143.

Régis, J., Mangin, J.-F., Frouin, V., Sastre, F., Peragut, J.C., Samson, Y., 1995. Generic model for the localization of the cerebral cortex and preoperative multimodal integration in epilepsy surgery. Stereotactic Funct. Neurosurg. 65, 72–80.

Rettman, M., Han, X., Xu, C., Prince, J., 2002. Automated sulcal segmentation using watersheds on the cortical surface. NeuroImage 15, 329–344.

Rivière, D., Mangin, J.-F., Papadopoulos-Orfanos, D., Martinez, J.-M., Frouin, V., Régis, J., 2002. Automatic recognition of cortical sulci of the human brain using a congregation of neural networks. Med. Image Anal. 6 (2), 77–92.

Serra, J., 1982. Image Analysis and Mathematical Morphology. Academic Press, New York.

Sowell, E., Thompson, P., Rex, D., Kornsand, D., Tessner, K., Jernigan, T., Toga, A., 2002. Mapping sulcal pattern asymmetry and local cortical surface gray matter distribution in vivo: maturation in perisylvian cortices. Cereb. Cortex 12, 17–26.

Talairach, J., Tournoux, P., 1988. Co-planar Stereotaxic Atlas of the Human Brain. Thieme Medical, New York.

Thompson, P., Cannon, T., Narr, K., van Erp, T., Poutanen, V., Huttunen, M., Lonnqvist, J., Standertskjold-Nordenstam, C., Kaprio, J., Khaledy, M., Dail, R., Zoumalan, C., Toga, A., 2001. Genetic influences on brain structure. Nat. Neurosci. 4 (3), 83–95.

Thompson, P., Toga, A.W., 1996. Detection, visualization and animation of abnormal anatomic structure with a deformable probabilistic brain atlas based on random vector field transformation. Med. Image Anal. 1 (4), 271–294.

Thompson, P.M., Woods, R.P., Mega, M.S., Toga, A.W., 2000. Mathematical/computational challenges in creating deformable and probabilistic atlases of the human brain. Hum. Brain Mapp. 9, 81–92.

Toga, A.W., Thompson, P.M., 2002. New approaches in brain morphometry. Am. J. Geriatr. Psychiatry 10 (1), 13–23.

Tzourio-Mazoyer, N., Landeau, B., Papathanassiou, D., Crivello, F., Etard, O., Delcroix, N., Mazoyer, B., Joliot, M., 2002. Automated anatomical labeling of activations in SPM using a macroscopic anatomical parcellation of the MNI MRI single-subject brain. NeuroImage 15 (1), 273–289.

Van Essen, D.C., 1997. A tension-based theory of morphogenesis and compact wiring in the central nervous system. Nature 385, 313–318.

Verwer, B.J.H., Verbeek, P.W., Dekker, S.T., 1989. An efficient uniform cost algorithm applied to distance transforms. IEEE PAMI 11 (4), 425–428.

White, L.E., Andrews, T.J., Hulette, C., Richards, A., Groelle, M., Paydarfar, J., Purves, D., 1997. Structure of the human sensorimotor system. I. Morphology and cytoarchitecture of the central sulcus. Cereb. Cortex 7 (1), 18–30.

Woermann, F.G., Free, S.L., Koepp, M.J., Ashburner, J., Duncan, J.S., 1999. Voxel-by-voxel comparison of automatically segmented cerebral gray matter—a rater-independent comparison of structural MRI in patients with epilepsy. NeuroImage 10, 373–384.

Yousry, T.A., Schmid, U.D., Alkadhi, H., Schmidt, D., Peraud, A., Buettner, A., Winkler, P., 1997. Localization of the motor hand area to a knob on the precentral gyrus. A new landmark. Brain 120 (1), 141–157.